AMERICAN METEOROLOGICAL SOCIETY

Journal of Applied Meteorology and Climatology

EARLY ONLINE RELEASE

The DOI for this manuscript is doi: 10.1175/JAMC-D-16-0167.1

Analysis of heat index in Mesoamerica and Caribbean Region

*Nazario D. Ramirez-Beltran
Department of Industrial Engineering,
University of Puerto Rico,
P.O. Box 9030, Mayagüez, PR 00681, U.S.A.
nazario.ramirez@upr.edu,

Jorge E. Gonzalez
Department of Mechanical Engineering,
The City College of New York,
140 the Convent Ave., New York, NY 10031,
gonzalez@me.ccny.cuny.edu

Joan M. Castro
Department of Civil Engineering,
University of Puerto Rico,
P.O. Box 9040, Mayagüez, PR 00681, U.S.A,
joan.castro@upr.edu

Moises Angeles
Department of Mechanical Engineering,
The City College of New York,
140 the Convent Ave., New York, NY 10031,
mangeles@ccny.cuny.edu

Eric W. Harmsen
Department of Agricultural and Biosystems Engineering,
University of Puerto Rico,
Mayagüez, PR 00680, U.S.A,
eric.harmsen@upr.edu

Cesar M. Salazar
Department of Industrial Engineering,
University of Puerto Rico,
P.O. Box 9030, Mayagüez, PR 00681, U.S.A,
cesar.salazar@upr.edu

* Indicates the corresponding author.

Abstract

Hourly data collected from ground stations were used to study the maximum daytime heat index (H_i) in the Mesoamerica and Caribbean (MAC) region for a 35-year period (1980-2014). Observations of the H_i revealed larger values during the rainy season and smaller values during the dry season. H_i climatology exhibits the largest values in Mesoamerica, followed by the Greater Antilles Islands and then by the Lesser Antilles Islands. The trend of the H_i indicates a notable increasing trend of 0.05 °C year^{-1} (0.10 °F year^{-1}), and the trends are more prominent in Mesoamerica than in Caribbean countries. This work also includes the analysis of heat index extreme events. Usually the extreme values of heat index are used for advising heat warning events, and it was found that 45 heat index extreme events (HIEE) occurred during the studied period. The average duration of HIEE was 2.4 days, and the average relative intensity (excess over the threshold) was 2.4 °C (4.3 °F). It was found that 82 % of HIEE lasted 2 or 2.5 days, and 80 % exhibited relative intensity of 3 °C (5.4 °F) or less. It was also found that the frequency of extreme events has intensified since 1991 with the highest incidences occurring in 1995, 1998, 2005 and 2010; and these years coincide with the cool phase of El Niño Southern Oscillation (ENSO). Therefore, the occurrences of HIEE in the MAC region appear to be at least partially influenced by ENSO episodes.

1. Introduction.

The heat index is the combination of air temperature and relative humidity (RH) and is an attempt to estimate what humans feel as an apparent temperature. The variation of heat index is linked to both human health and energy demands to maintain indoor room comfort (González-Cruz et al. 2013) and hence it is important to characterize the behavior of the heat index. This index is based on the human energy balance and was determined as the result of various extensive

biometeorological studies (Fanger 1970; Steadman 1979; Rothfusz 1990). The human body usually adapts to hot temperatures by perspiration, when heat is removed from our body by sweat evaporation. High values of RH reduce the evaporation rate causing lower heat removal from our body and hence the sensation of being overheated. Steadman (1979) studied the human response under different environmental conditions to derive a theory for estimating the apparent temperature or heat index. His method takes into account the effects of air temperature and RH on the reaction of the human body and expresses the physiological reaction, clothing resistance, moisture content, and heat-transfer interactions as an apparent temperature. Steadman's work was based on the human biometeorology study conducted by Fanger (1970) who measured the reaction of 256 adults wearing different clothing and performing various physical activities under certain environmental conditions. Fanger's experiments provided the basis for deriving physiological data describing the average heat and moisture transfer. Steadman (1979) derived a method to estimate the apparent temperature based on the amount of heat lost via exhaling and the skin's resistance to heat and moisture transfer. Rothfusz (1990) used Steadman's results to develop a regression equation, which expresses the relationship between temperature at different RH and the skin's resistance to heat and moisture transfer. The United States National Weather Service (NWS) developed its own algorithm for estimating heat index based on Steadman's and Rothfusz's work. This method was adopted and it is available online (NOAA/NWS, 2016) with a detailed description of the algorithm given by Anderson et al. (2013).

Dixon (1998) reported the heat index climatological conditions in the southern United States, and pointed out that the climatological conditions can be used to evaluate the forecasted heat index severity and assisting the issuance of hazardous heat advisories. It is known when the heat index is greater or equal to 40.5 °C (105 °F) the warmer environment is dangerous and can

potentially cause heat cramps and heat stroke when exposure is prolonged in combination with physical activity (NWS, 2016). Dixon (1998) reported 10 years (1980 - 1989) of summertime daily air temperature and RH data for 40 stations. New Orleans recorded the largest heat index 51.1 °C (124 °F). Rakib (2013) presented the temporal variation of extreme temperatures in Bangladesh. The variables considered in this study include average seasonal maximum and minimum air temperature, RH and maximum heat index. Daily records were obtained from 18 meteorological stations during the period (1981 – 2010). Rakib (2013) observed a significant increase in air temperature in the past decades, especially along the coastal and central areas of Bangladesh. A larger maximum heat index was also observed during the wet season.

The National Weather Service (NWS) issues an "Excessive Heat Warning" (NWS, 2017) when the maximum heat index temperature is expected to be 40.6 °C (105 °F) or higher for at least two days and night time air temperatures will not drop below 21.1 °C (75 °F). However, these criteria vary across the country, especially for areas not accustomed to extreme heat conditions. Robinson (2000) suggested that heat watches and warnings are issued when the heat index is greater than or equal to 40.6 °C (105 °F) during the daytime and greater than or equal to 26.6 °C (80 °F) at nighttime for at least two consecutive days. Thus, the HIEE can be used to anticipate the potential occurrence of a heat wave.

A heat wave is a persistent period of having a significant temperature deviation from the normal climate conditions of a given region, and consequently a heat wave can occur in a region with either hot, warm, or cold climate. In general, every location has its own and unique climatology of heat, and consequently, there are several definitions of heat waves, but all of them include some notions of persistent extreme high temperature. The World Meteorological Organization defines a heat wave as the event when daily maximum temperature exceeds the

average maximum temperature by 5 ℃ (9 ℉) for more than five consecutive days, where the normal period is from 1961 to 1990 (MetOffice, 2015). In the United States the heat wave is defined as a period of at least two consecutive days of excessively hot weather (NWS, 2015). In the northeast, which is characterized by having high humidity, a heat wave is three consecutive days where temperatures reach or exceed 32.2 ℃ (90℉). In dry zones, the heat wave occurs when temperature reaches 37.8℃ (100℉) for three or more consecutive days. The HIEE is a different phenomenon from the heat wave, since the heat wave requires persistent high temperatures; whereas, the HIEE requires persistent high temperatures, which are combined with observed RH values.

According to the authors' knowledge there is no published scientific studies of heat index over the MAC region, however, studies do show that extreme episodes of heat index are triggering serious public health issues in most mid-latitude and continental cities (Wang et al. 2012; Loughnan et al. 2014; Méndez-Lázaro et al. 2015; Portier et al. 2010). Therefore, this paper focuses on understanding the climatology and trends of the H_i, as well as analyzing the extreme events in terms of duration, intensity and frequency in the MAC region. The second section explains what types of data were used. The third section describes the methodology, which includes the major challenges encountered when dealing with weather station data, a general overview of the MAC climate characteristics, the analyses of H_i as well as the characterization of HIEE. The fourth section presents analysis of results, which are organized in three parts: station characteristics, H_i trends and climatology, and analysis of extreme events. The last section includes a summary of the work and conclusions.

2. Data

Two types of data were used in this research, reanalysis data and observations from weather stations. The source of the first type of data was the National Centers for Environmental Prediction (NCEP) Reanalysis. Thirty-five years (1980 – 2014) of 6-hourly data were used for estimating the MAC climate characteristics, and describe the spatial variability of the regional H_i pattern (NCEP 2016). The NCEP reanalysis data include the following domain from 0 °N to 30 °N and 60 °W to 100 °W which correspond to (13 x 18) 234 grids with 2.5 ° by 2.5 ° resolution. NCEP reanalysis data are developed by using a state-of-the-art analysis/forecast system to perform data assimilation using global past data from 1948 to the present. Thus, there are systematic differences between NCEP reanalysis and observational datasets (ESRL 2016). For a given grid data NCEP represents the average value for a relatively large area of a specific variable; whereas, a station observation is a measurement of a single point. Hence, temperatures and RH from NCEP reanalysis data are expected to be different from station measurements. However, NCEP data simplify calculations, since there are no missing values, and provide the opportunity of deriving insight about the behavior of meteorological variables.

Thirty-five years (1980 - 2014) of hourly data from 15 ground stations were also used to perform H_i analyses. The source for weather station data is the National Center for Environmental Information (NCEI 2016), which also includes the Global Historical Climatology Network (GHCN). The MAC region station data are mostly limited by the availability of observations of dew point temperature over 35 years. The characteristics of the Caribbean and Mesoamerica stations, along with the percentage of data for each station are given in Table 1. This table also includes the original and filtered data, after applying data quality control. The MAC region (5 °N to 30 °N and 90 °W to 60 °W) includes the Caribbean that is divided into the Lesser and Greater

Antilles islands, and Mesoamerica includes parts of Mexico, Central America and the North part of South America, as shown in Figure 1.

3. Methodology

The applied methodology in this research includes five major tasks to develop the strategy for accomplishing the objectives of this work: a). evaluate the quality of the weather station data; b). use NCEP data to obtain climate characteristics of the MAC region; c). present the heat index definition, and its 24-hour climatology; d). describe the techniques for computing trends and climatology patterns of H_i; and e). describe the analysis of the HIEE..

a. Data quality control

Ground station data recorded the real and inherent behavior of the atmosphere and revealed the actual climate patterns and variability. However, working with long-term ground station records is challenging since each individual station is accompanied by their own set of inherited obstacles. For example, the types of instruments used vary since they belong to different countries. The observations were collected at different frequencies 1, 3, or every 6 hours. It should be noted that the frequency of data collection affects the accuracy on the calculation of the H_i. Observations during daytime are more abundant than during nighttime. Some stations show inconsistency on frequency of data collection.

A homogeneous climate time series is defined as one where variations are caused only by alteration in weather and climate (Peterson et al. 1998a). Thus, inhomogeneous climate data includes errors such as drift, jumps, and change in variability, etc. These types of error are associated with change of instruments, non-calibration, station moves, urbanization, different observation times, human errors; etc. The inhomogeneities can bias a time series and lead to misinterpretations of the studied climate (Peterson et al. 1998b). There are several algorithms and

177 strategies that help in detecting and fixing the inhomogeneity features in climate data
178 (Alexandersson 1986; Peterson et al. 1998a; 1998b; Reeves et al. 2007; Gallagher et al. 2013;
179 Menne et al. 2009).

180 A request for information regarding the location and equipment history of the studied
181 stations was submitted; however, no information corresponding to the NCEI stations was found.
182 The available statistical tools usually work with a station, which is surrounded by similar stations,
183 and the available observations from the nearby stations are used to remove the inhomogeneities of
184 the station in question (Peterson et al. 1998a; 1998b; Reeves et al. 2007). Air and dew point
185 temperatures were collected from weather stations mostly located at the international airports. Due
186 to the long-term duration of these data, several of the datasets contained inhomogeneities. The
187 stations that provided the required data for this study are isolated weather stations; and
188 consequently, conventional tools are non-applicable for treating inhomogeneous time series.
189 However, an alternative method was developed in this work and consists of removing values that
190 are not likely to belong to a given climate data. Thus, the implemented approach for each station
191 includes five steps:

192 1) REMOVE INSUFFICIENT DATA.

193 Data were organized for each hour and 24 time series were created. One series was created
194 with daily observations at 0:00 UTC, the second series at 1:00 UTC, etc., until completing the 24^{th}
195 time series at 23:00 UTC. These series are called Hour-Daily (HD) time series, and each complete
196 time series includes 12,784 HD observations. Therefore, any HD time series that has more than
197 75 % of missing values was removed from the data set, because of insufficient data to be analyzed.
198
199

2) REMOVE HOURLY INCONSISTENT DATA.

An inconsistent value is defined as a value that is not likely to belong to the majority of the values of a given climate dataset. One approach for detecting inconsistent data is to use the Chebyshev's inequality (Rohatgi 1976). The advantage of using Chebyshev's inequality is that it is a robust approach for detecting inconsistent data and does not require knowledge of the probability distribution of the underlying climate data. Chebyshev's inequality can be expressed as follows:

$$P(|x_i - \mu_i| > k\sigma_i) \leq \frac{1}{k^2} \quad (1)$$

where P is the probability statement, μ_i and σ_i are the mean and standard deviation of the climate data x_i (air or dew point temperatures) at the i^{th} station, and $k > 1$. As a result, any value that falls outside of this interval ($\mu_i \pm k\sigma_i$) is unlikely to be a real observation and will be declared as an inconsistent record. Any value satisfying the aforementioned condition was removed from the data set. Thus, an inconsistent value may be detected by using a k value between 3 to 5. A k value of 3 was selected since it provided satisfactory results. As the value of k is reduced, the screening procedure becomes more restrictive. The Chebyshev's probability statement indicates that for a k value of three 89 % or more of the selected data are likely to correspond to the actual observed climate data. The mean and standard deviation for each HD time series were estimated using the total number of available observations for the underlying time series. Inconsistent data were considered as missing values and were not estimated in order to avoid deriving fictitious results and incorrect conclusions.

3) REMOVE 24-HOUR INCONSISTENT DATA.

This rule consists of removing any value where the difference in temperature for the preceding or following day was greater than 25 °C (77 °F). Hence, searching for inconsistent data

223 was computed by using the following calculation$|x_t - x_{t-1}| > 25$ °C (77 °F), were t is the
224 corresponding time index for the HD time series.

225 4) REMOVE JULIAN DAY INCONSISTENT DATA.

226 Data were organized as follows: First, select the observed value at 0:00 UTC from the first
227 Julian day and from 1980. Second, select the observed value at 0:00 UTC from the first Julian day
228 and from 1981, and repeat the process until collecting the last observation at 0:00 UTC from the
229 first Julian day and from 2014. At this stage, the first of 35 observations are completed. The
230 second series was created by repeating the previous steps but now using the second Julian day.
231 Thus, the last series at 0:00 UTC will be created by repeating the previous steps and using now the
232 365th Julian day. Now, the process is repeated at 1:00 UTC to create others 365 series and each
233 one has 35 observations. The previous steps are repeated again at 2:00 UTC, and so on, until
234 completing the last series at 23:00 UTC. These series are defined as Hour-Julian day (HJ) time
235 series. Chebyshev's inequality was used to detect inconsistent values in each series, and the mean
236 and standard deviation were computed for each of the HJ time series.

237 5) FINAL ELIMINATION OF INCONSISTENT DATA.

238 The hourly data were reorganized in the original format and Chebyshev's inequality was
239 again used to remove inconsistent data. The average and standard deviation were computed using
240 all of the filtered data. Table 1 shows the percentage of original and the filtered data, and Figure
241 2 shows the original and the filtered data for stations located in Antigua & Barbuda, Cuba, and
242 Venezuela. These stations represent examples for the Lesser and the Greater Antilles, and
243 Mesoamerica, respectively. This figure shows the values that are not likely to belong to real
244 observations were subsequently and successfully removed using Chebyshev's inequality.
245

246 *b. Mesoamerica and Caribbean climate characteristics*

247 The MAC region is characterized by receiving intense solar irradiance every day due to the
248 proximity to the Earth's Equator. The climatology analyses in this section are based on daily
249 averages of 6-hourly data extracted from NCEP during the studied period. The H_i in this section
250 was computed using the maximum of the 6-hourly data of air temperature and the corresponding
251 RH. The average over the entire period and the annual trend were computed for every grid.

252 The climatology of air temperature follows a unimodal distribution receiving the largest
253 air temperature in August and the smallest in January (Figure 3. a). The H_i climatology follows
254 a similar pattern of daily maximum air temperature (T_{max}) and is given in Figure 3. b). The
255 climatology of the RH follows a bimodal distribution and starts ascending in March until reaching
256 the largest peak in June and the second peak occurs during the months of September through
257 October and starts descending until completing the cycle in March (Figure 3. c). This follows the
258 reported rainfall bimodal climatology for the Caribbean (Angeles et al. 2010) and the observed
259 RH. The rainfall increases humidity during rainy season and decreases during dry season. The
260 ocean increases the RH due to evaporation and moisture advection, which brings large humidity
261 to the MAC region. The average spatial distribution shows that temperatures reach the largest
262 values over the ocean and the RH shows the largest values over the Mesoamerican region (Figures
263 3d) and f). The spatial distribution of averages and trends of H_i were computed and are exhibited
264 in Figures 3e) and g), respectively. The largest H_i over land area are observed in Mexico (Yucatan
265 Peninsula), Cuba, Haiti, Jamaica and Puerto Rico. On the other hand, the largest increasing trends
266 of the H_i over land area are exhibited in Lesser Antilles followed by the Greater Antilles.

267 Precipitation is primarily affected by troughs imbedded in easterly waves during the rainy
268 season (May to October), generating large amounts of rainfall in the Caribbean basin. In addition,

subsidence from Central America, the Southern Oscillation by means of vertical wind shear, wind divergence, North Atlantic Oscillation and Saharan dust all contribute to the day to day rainfall variations (Goldenberg at al. 2001; Giannini et al. 2001; Jury 2015.). Cold fronts generate large cloudy areas and precipitation during winter months. The confluence of these synoptic scale events causes the Caribbean rainy season to follow a bimodal distribution (Angeles et al. 2010), dividing the season in the early rainfall season (May - July) and late rainfall season (August – October), with a short drought period in July. The first rainfall peak occurs in May and the second in September. The lowest amount of precipitation in the Caribbean occurs from December to March and it is known as the dry season.

c. Estimation of the Heat Index and 24-hour climatology

Robinson (2000) defines heat index as the combination of ambient temperature and RH that approximate the environmental aspect of the thermal regime of a human body. There are several methods to estimate heat index. Anderson et al. (2013) investigated the performance of 21 different algorithms under U.S. weather conditions. They used daily 2011 weather data, including mean air temperature, mean dew point temperature, and mean RH, in all 50 U.S. state capitals. They analyzed whether each algorithm produced heat index values consistent with Steadman's original apparent temperature (Steadman 1979) and found that the algorithms were inconsistent across studies. They concluded that the NWS algorithm provides reproducible and consistent environmental results. In this work, we adopted the NWS approach described in Anderson et al. (2013).

Typically, temperature and RH are combined to develop short-term heat index forecasts with the goal of providing heat waring to the society. The approach used in this work is different from the standard use of heat index, in the sense that we are using information from a station to

292 calculate the heat index; and climatology and trends are based on 35 years of hourly data.
293 However, we adopted the standard algorithm to calculate the heat index (NWS, 2016; Anderson
294 et al. 2013).

295 Usually, stations reported hourly data during daytime, and consequently H_i at a given
296 station was calculated using the maximum of hourly air temperature recorded during the hours
297 from 10:00 UTC to 22:00 UTC, and the dew point was selected at the time when the T_{max} occurred.
298 This time interval was selected because H_i is most likely to occur during daytime hours. The 24-
299 hour climatology was calculated by computing the average for every hour during the 35 years of
300 data. The 24-hours climatology indicates that maximum H_i corresponds to the T_{max} and
301 approximately the minimum of RH; whereas, the minimum H_i corresponds to the minimum air
302 temperature and about the maximum RH, shown in Figure 4. This figure exhibits 24-hours average
303 heat index behavior of three stations: Antigua-Barbuda station (top; 17.137 °N, 61.793 °W),
304 Puerto Rico station (center; 18.417 °N, 66 °W), and Colombia station (bottom; 10.89 °N, 74.781
305 °W). These stations correspond to a sample from the Lesser and Greater Antilles, and
306 Mesoamerica zone, respectively.

307 *d. Trends and climatology of Maximum Daytime Heat Index*

308 The climatology patterns and characteristics of each station were organized into
309 homogenous climate zones to best represent the H_i seasonal variability over different geographical
310 zones and to conduct proper analyses. The self-organizing feature maps (SOFM) was used to
311 identify the homogeneous climatological patterns. The SOFM is an artificial neural network that
312 uses an unsupervised competitive learning algorithm to organize a set of data into homogenous
313 classes (Hagan et al. 2014; Yip and M.K. 2012; Ultsch and Roske 2002). The SOFM suggests that
314 the data can be organized in 3 homogenous groups and correspond to the different geographical

zones. The homogeneous groups were located in: Lesser Antilles Islands, Greater Antilles Islands, and Mesoamerica coastal zone. Figure 1 indicates the weather station locations, with the majority of stations located in the coastal areas, and the dotted red line in Figure 1 shows the identified homogenous zones. The SOFM included Miami, Florida USA (station 12) and Honduras (station 10) within the Greater Antilles zone since their climatological characteristics resemble inherent properties associated to this zone.

The annual time series of a given climate variable usually exhibit an increasing or decreasing trend that is typically represented by a linear function. The slope of the linear function is estimated by parametric or nonparametric methods. The usual parametric method is the least square method and one of the nonparametric techniques is the Theil-Sen method (Zaman et al. 2015). The nonparametric method is robust to the presence of outliers and both methods are affected by the autocorrelation of the underling time series. Hence, the slope significance is sensitive to the presence of the autocorrelation of the climate data. It is known that when the autocorrelation of the time series is high the t-statistic associated with the slope is overestimated and consequently the significance of the slope is also overestimated. To avoid this problem, the autocorrelation of the data should be parameterized and included in the regression model (Abraham and Ledolter 2006).

Assuming the studied climate time series have moderate autocorrelation, a linear regression methodology was applied for computing trends, and the daily averages were used to calculate the climatology for the H_i. A straight line was fitted to the H_i to measure the trend. The slope of the straight line was tested to determine whether or not it is statistically significant. Daily heat indices were also aggregated to compute monthly and annual time series to estimate trends. Data were

337 also aggregated for homogenous zones to estimate trends for Lesser and Greater Antilles Islands
338 and also for the Mesoamerica zone.

339 *e. Analysis of heat index extreme events*

340 In the MAC region, it is common to find places with extreme hot behavior during daytimes.
341 However, the critical weather condition occurs when the hot conditions are also maintained during
342 night times. Therefore, *the HIEE in the MAC region is defined as an extraordinary hot event*
343 *where the maximum-daytime heat index and the minimum-nighttime heat index both exceed the*
344 *corresponding 97th percentiles and this hot event must persist for at least two consecutive days*.
345 The 97th percentiles should be derived with the analysis of at least 30 years of hourly data, and this
346 percentile was determined after computing all the potential extreme heat events based on a "*q*"
347 percentile, where "*q*" varies from 95 to 99 with increments of one. A HIEE must be a rare event
348 and according to the NWS (Robinson 2000), is such that a station should have less than 3 extreme
349 heat events per decade. Thus, an approximation of a rare event definition for the MAC region
350 would be a station that has 10 or less HIEE during 3.5 decades, and the corresponding percentile
351 that meets this criterion was the 97th. Greater than the 97th percentile was not selected because
352 some important hot-humid events may be missing. Since, when a high percentile is applied it is
353 difficult for the event to maintain the hot and humid levels during two days to qualify for extreme
354 event. On the other hand, less than 97th percentile was also not selected because it does not
355 correspond to the rare event criterion.

356 Table 4 shows the number of extreme hot events for each station when the percentile varies
357 from 95 to 99. Thus, the 97th percentile is the one that meets the rare event criterion and detects
358 extreme events. This percentile provides 45 extreme events for the region, and it is enough data
359 to perform analysis of the extreme events.

4. Results

Results for analyzing the H_i in the MAC region were organized in three parts: the first part describes the climate characteristics of the stations and also the characteristic for each homogenous region. The second part presents results of trend analysis and climatology patterns of H_i, and the third part presents the analysis of heat index extreme events.

a. Station climate characteristics

Table 1 summarizes the climate characteristics for each of the studied stations. In each country, the station that provides the most complete data set was selected and the largest sample size was found at the Miami International Airport (12,695 days) and the smallest in Guadeloupe (9,068 days). The station that exhibits the largest T_{max} average was La Chinita International Airport in Venezuela (32.8 °C, 91 °F); whereas, the station with the lowest air temperature average was located at the Miami International Airport (28.6 °C, 83.4 °F). This result was expected since these stations are located at about sea level and Miami is at the highest latitude (25.8 °N) and La Chinita at the lowest latitude (10.6 °N). The station Le Raizet located in Guadalupe shows the highest average RH of 69.8 %, and the station Toussaint Louverture at the International airport located in Haiti exhibited the lowest average RH (51.4 %). The station La Chinita International Airport in Venezuela shows the largest average H_i (38.3 °C, 100.9 °F); whereas the station at the Miami International Airport shows the smallest average of H_i (31 °C, 87.8 °F). This result was expected because temperature has a greater influence than RH on H_i. The difference between H_i and the T_{max} was computed. The largest difference (6.2 °C, 11.2 °F) was reported in Ernesto Cortissoz station located in Colombia. The average temperature of La Chinita is larger than temperature in Ernesto Cortissoz, and it was expected that the largest difference should be found in Chinita. However, the RH humidity is larger in Ernesto Cortissoz and it caused the largest

difference at Ernesto Cortissoz. On the other hand, the smallest difference (2.4 °C, 4.3 °F) was found at the Miami International airport station, since the temperature was the dominant parameter in the estimation of heat index.

Table 2 shows a summary of the characteristics of each of the Mesoamerican and Caribbean zones, and includes the averages of sample size, T_{max}, RH, H_i average, and average of the difference between H_i and T_{max}. The Lesser and Greater Antilles islands exhibited similar characteristics, except for RH, the Lesser Antilles islands showed on average the largest RH since they are very small islands with intense rainfall and ocean evaporation dominates in this zone. In terms of T_{max}, the averages for the Lesser and Greater Antilles were almost the same, having the smallest average maximum air temperature (29.4 °C, 84.9 °F) in the studied area, while the Mesoamerica zone exhibits the largest average of T_{max} (31.7 °C, 89 °F). The Greater Antilles exhibit the smallest difference ($H_i - T_{max}$), about 3.4 °C (6.1 °F). On the other hand, the Mesoamerica zone showed the largest averages of H_i, T_{max}, [37.1 °C (98.8 °F), 31.7 °C (89 °F)] and the largest difference (5.4 °C, 9.8 °F). Thus, it is likely that people living in Mesoamerica countries are exposed to a higher risk than those living in the Caribbean countries (NOAA/NWS 2016; OSHA 2016).

b. Trends and climatology

The T_{max} time series are shown in Figure 5 panel a), while panel b) shows the H_i for the MAC region based on stations data. A linear trend was computed for each of the time series and significant trends were observed: T_{max} and H_i of $0.02\ ^{\circ}C$ year^{-1} (0.04 °F year^{-1}), and $0.05\ ^{\circ}C\ year^{-1}$ (0.10 °F year^{-1}), respectively. Trenberth et al. (2007) and Jury (2015) reported a similar temperature trend for the Caribbean and Puerto Rico, respectively. The trend and climatology for the RH are given in Figure 5 panels c) and d), respectively. Panel c) shows that

406 RH has some fluctuation around the mean with no significant trend. Panel d) shows that the
407 climatology of the RH follows a bimodal distribution and starts ascending in March until reaching
408 the first peak in June with a small reduction in July. The largest peak occurs in November and
409 starts descending until completing the cycle in March. Angeles et al. (2010) show that the
410 Caribbean rainfall climatology exhibits a small reduction in July and they claim that the rainfall
411 bimodal behavior is influenced by the vertical wind shear and the aerosol particles. Thus, it is
412 likely that the RH bimodal pattern is also influenced by the above-mentioned variables. Panel e)
413 in Figure 5 exhibits the climatology of T_{max} and this pattern is similar to the H_i climatology. The
414 panel f) in Figure 5 shows the climatology of H_i for the entire region, and follows a unimodal
415 distribution. The H_i reduction observed in July is caused by the reduction in RH and the largest
416 peak in H_i is also caused by the increase in RH; however, the largest value in H_i occurred earlier
417 than the peak in the RH, because the air temperature is the dominant variable and starts decreasing
418 in September. . Panel g) in Figure 5 shows the difference between H_i and T_{max} for the entire
419 region and exhibits a similar pattern to the H_i. The difference between H_i and T_{max} varies between
420 2 °C (3.6 °F) in January and 6 °C (10.8 °F) in August. These analyses show how the potential
421 period for extreme hot events are more likely to take place during the rainy season and less likely
422 to occur during the dry season. This observation is in agreement with reports presented in other
423 parts of the world (Dixon 1998; Rakib 2013).

424 Figure 6 and 7 show the T_{max} and H_i trends for the three MAC zones, respectively. The
425 trends for T_{max} and H_i in each zone are given in Table 3, which indicates that in the Lesser Antilles
426 the trends of T_{max} and H_i are significant and show increasing trends of 0.02 °C year^{-1} (0.03
427 °F year^{-1}) and 0.04 °C year^{-1} (0.08 °F year^{-1}), respectively. In addition, the trends for both the
428 T_{max} and H_i in Mesoamerica are significant with a large rate of 0.06 °C year^{-1} (0.11 °F year^{-1})

and 0.16 °C year^{-1} (0.29 °F year^{-1}), respectively. However, the trends for the maximum temperature and heat index in the Greater Antilles are not significant, as shown in Table 3. In addition, Figure 8 and Table 3 show that RH has no significant trend, with the exception of the Lesser Antilles, exhibiting a reduction of 0.09 % per year.

The climatology of T_{max}, RH, and H_i are shown in Figure 9. It is noted that climatology for each of the following variables T_{max} and H_i follows a bimodal distribution for Mesoamerica; however, a unimodal distribution is shown for the Caribbean islands (Lesser and Greater Antilles). On the other hand, the climatology for the Lesser Antilles show the largest RH with the smallest H_i, since its T_{max} values are about the smallest over the entire studied region. The climatology of the RH follows a bimodal distribution and starts ascending in March until obtaining the first peak in June or in July followed by a small reduction and then continues rising until achieving the maximum peak in October or in November (bottom panel in Figure 9). It can be observed that the Mesoamerica region is the hottest zone followed by the Greater Antilles and then the Lesser Antilles. On the other hand, the Lesser Antilles islands revealed the largest RH, followed by Mesoamerica, and the smallest RH (during summer) is in Greater Antilles.

c. Analysis of heat index extreme events

Observations collected during 10 to 22 UTC were associated with daytime events; whereas observations that fall outside this range were used to identify nighttime hot events. Based on 35 years of hourly data, the maximum and the minimum thresholds for each station were computed, and they are shown in Table 5. The threshold for each station varies since each station exhibits different local climatological conditions. On average Mesoamerican countries exhibit the hottest events (>46.0 °C, 114.8 °F) during the daytime. The Lesser Antilles exhibits the hottest nighttime events (>30.7 °C, 87.3 °F). The difference between the average daytime and nighttime thresholds

452 are greatest (17.5 °C, 31.5 °F) in Mesoamerica and the smallest (8.1 °C, 14.6 °F) in the Lesser
453 Antilles. A practical contribution of this work is to suggest thresholds for identifying the
454 occurrence of HIEE in the MAC region.

455 The major characteristics of the HIEE are the duration (d) and the intensity, which are the
456 parameters that determine the severity of the hot events. For a given station, the relative intensity
457 (ri) was used to perform analysis (instead of absolute intensity) since the intensity depends on the
458 local climate characteristics. The relative intensity is the number of degrees that the maximum
459 heat index exceeds the threshold (or 97^{th} percentile) of a given station; whereas, the absolute
460 intensity is the actual intensity observed at a station. The relative intensity was used to be able to
461 compare the strength of HIEE that occurs for different climate conditions. Thus, to characterize
462 the severity of an extreme hot event, it is required to jointly study the duration and intensity of the
463 event, and the joint probability distribution is given in Table 6 and in Figure 10.

464 The correlation between duration and relative intensity is 0.19 indicating that there is a
465 weak linear dependency between these variables. Although, the correlation is weak the analysis
466 of HIEE should be performed using simultaneous duration and relative intensity, since a nonlinear
467 dependency may exist between these variables. The joint probability distribution can be used to
468 answer practical questions related to the duration and intensity of a given HIEE. For instance,
469 what would be the possibility that an extreme event will last 3 or less days with a relative intensity
470 equal or less than 3 °C (5.4 °F)? The joint probability distribution indicates that 71% of the
471 extreme events in the MAC region meet these conditions.

472 The joint probability distribution suggests that a severe HIEE occurs when the relative
473 intensity is greater than 3 °C (5.4 °F) and persists for more than 4 days, and the probability of this

event to occur is 0.022. Only one event out of 45 extreme events occurred during the 35 year study period, in September 2009 in Antigua & Barbuda and lasted 4.5 days and a 4 °C (7.2 °F) relative intensity. On the other hand, the most likely HIEE is the one that shows a relative intensity less than 3 °C (5.4 °F) with duration less than 3 days, and the probability of this event to occur is 0.55.

The last column of Table 6 shows the marginal duration probability distribution of HIEE; whereas, the last row exhibits the marginal probability distribution of relative intensity. It was found that the average duration of heat index extreme event was 2.43 days and standard deviation of 0.57 days. The mean of relative intensity was 2.44 °C (4.39 °F) and standard deviation of 1.22 °C (2.20 °F). The duration probability distribution indicates that 82% of heat events last less than 3 days, and the relative intensity distribution shows that 80% of heat events exhibit a relative intensity less than 4 °C (7.2 °F).

The third important characteristic of the HIEE is the annual and monthly frequencies. Figure 11 a) shows that the annual frequency of extreme events has intensified since 1991, with the highest incidences recorded in 1995, 1998, 2005 and 2010, and these years coincide with the occurrence of ENSO, and especially during its cool phase (NOAA/ONI, 2017). Figure 11 b) indicates that the HIEEs have occurred during the rainy season with the largest frequency occurring in August. During the rainy season in the years 1982 and 1987 El Niño events were very strong and moderate, respectively; but their effects were not reflected in the frequency of the HIEEs. Hence, the frequency of HIEE in the MAC is partially modulated by ENSO. Additional research is needed to identify the remaining factors that contribute to develop HIEE.

5. Summary and Conclusions

Ground stations data were used to estimate the heat index over the Caribbean and Mesoamerican Region during 35 years. Daily H_i was computed based on hourly observations of air temperature and RH. The H_i trend shows a notable increase during the studied period. The trend of the heat index is more prominent in Mesoamerica than in Caribbean countries.

Values of H_i were higher in Mesoamerica, followed by the Greater Antilles Islands and then by the Lesser Antilles Islands. Climatology of H_i follows a unimodal distribution for the entire Caribbean Islands with the largest values occurring in August. Mesoamerica countries exhibited a bimodal H_i distribution with the first peak in May and the second in August. The climatology of the RH in the MAC region follows a bimodal distribution with the largest peak in June and the second peak occurs during the months of October to November with the smallest RH occurs in March. In the MAC region the RH exhibits fluctuations about the mean with no significant trend. The climatology of the H_i ranges from 30 °C (86 °F) to 37 °C (98.6 °F), the RH varies from 60 % to 67 %, and the T_{max} range from 28 °C (82.4 °F) to 32 °C (89.6 °F).

The HIEE in the MAC region is defined as an extraordinary hot event where the maximum-daytime heat index and the minimum-nighttime heat index both exceed the corresponding 97th percentiles and this hot event must persist for at least during two consecutive days. The average threshold for the minimum and the maximum heat index for the Lesser Antilles Islands are 30.7 °C and 38.8 °C (87.3 °F and 101.8 °F); for the Greater Antilles Islands are 27.7 °C and 40.2 °C (81.9 °F and 108.0 °F); and for Mesoamerica are 28.5 °C and 46.0 °C (83.3 °F and 114.8 °F), respectively. On average, Mesoamerican countries exhibit the hottest daytime events (>46.0 °C, 114.8 °F) and the Lesser Antilles exhibit the hottest nighttime events (>30.7 °C, 87.3 °F). On

518 average the difference between the daytime and nighttime thresholds is greatest in Mesoamerica
519 (17.5 °C, 31.5 °F) and smallest in the Lesser Antilles (8.1 °C, 14.6 °F).

520 The duration and relative intensity of HIEEs were used to characterize these events. The
521 severity of a HIEE cannot be determined just by looking the duration of the relative intensity alone.
522 It is necessary to observe the strength of both variables simultaneously; i.e., it is recommended to
523 use the joint probability distribution to estimate the likelihood that a HIEE develops at a certain
524 level of strength.

525 The correlation between duration and relative intensity is 0.19 indicating that there is a
526 weak linear dependency between these variables. Although, the correlation is weak the analysis
527 of HIEE should be performed using simultaneously duration and relative intensity, since a
528 nonlinear dependency may exist between these variables. The joint probability distribution
529 suggests that a severe HIEE occurs when the relative intensity is greater than 3 °C (5.4 °F) and
530 persists for more than 4 days, and the probability of this event to occur is 0.022. Only one event
531 out of 45 extreme events occurred during the 35 year study period, in September 2009 in Antigua
532 & Barbuda and lasted 4.5 days and a 4 °C (7.2 °F) relative intensity. On the other hand, the most
533 likely HIEE is the one that shows a relative intensity less than 3 °C (5.4 °F) with duration less
534 than 3 days, and the probability of this event to occur is 0.55.

535 The annual frequency of HIEE has intensified since 1991 and the years with high
536 incidences coincide with the cool phase of ENSO. However, there were a few years when ENSO
537 episodes occurred and their effects were not reflected in the frequency of the HIEEs.
538 Consequently, additional research is needed to better understand the climate parameters that
539 control the annual frequency of HIEE.

It should be noted that this study is limited in the sense that no validation was perform with health-related data, and no comparison was conducted with other thermal stress.

Acknowledgements

This work was supported primarily by National Science Foundation (NSF) under the Environmental Engineering program with the grant CBET-1438324 and by The National Oceanic and Atmospheric Administration: Cooperative Remote Sensing Science and Technology Center (NOAA-CREST) under grant NA11SEC4810004, and by the University of Puerto Rico. The authors appreciate the excellent contribution from anonymous reviewers that motivate to significantly improve the manuscript.

References

Abraham, B., and J. Ledolter, 2006: *Introduction to regression modeling*. Thomson Brooks/Cole, 433 pp.

Alexandersson, H., 1986: A homogeneity test applied to precipitation data. *J. of Climatol.*, **6**, 661-675.

Anderson, G.B., M.L. Bell, and R.D. Peng, 2013: Methods to Calculate the Heat Index as an Exposure Metric in Environmental Health Research. *Environmental Health Perspectives*, **121**, No 10, 1111-1119.

Angeles, M.E., J. E. González, N. D. Ramírez-Beltrán, C. A. Tepley, and D. E. Comarazamy, 2010: Origins of the Caribbean Rainfall Bimodal Behavior. *J. Geophys. Res*., **115**, D11106, doi:10.1029/2009JD012990.

Dixon, R.W., 1998: A Heat Index Climatology for the Southern in United States. *National Weather Digest*, **22**, Number 1, 16-21.

ESRL, 2016: Earth System Research Laboratory. Accessed on October 11, 2016, [Available online at http://www.esrl.noaa.gov/psd/data/gridded/data.ncep.reanalysis.html#temp]

Fanger, P.O., 1970: *Thermal Comfort*. Danish Technical Press, 244 pp.

Gallagher, C., R. Lund, and M. Robbins, 2013: Changepoint Detection in Climate Time Series with Long-Term Trends. *Journal of climate*, **26**, 4994-5006.

Giannini, A., Y. Kushnir, M.A. Cane, 2001: Seasonality in the impact of ENSO and the North Atlantic high on Caribbean rainfall. *Phys. Chem. Earth* Part B, **26** (2001), 143–147.

Goldenberg, S.B., C. W. Landsea, A. M. Metas-Nunez, and W. M. Gray, 2001: The Recent Increase in Atlantic Hurricane Activity: Causes and Implications. *Science*, **293**, 474-479.

González-Cruz, J., P. Sequera, Y. Molina, R. Picon, J. Pillich, A. T. Ghebreegziabhe, and B. Bornstein, 2013: Climate and Energy Vulnerability in Coastal Regions: The Case for US Pacific and Northeast Corridor Coastal Regions. *Climate Vulnerability: Understanding and Addressing Threats to Essential Resources*, Elsevier Inc., Academic Press, 3–35.

Hagan, M.T., Demuth, H.B., M. Beal, and O. De Jesus, 2014: *Neural Network Design*, second edition, PWS Publishing Co., 800 pp.

Jury, M.R., 2015: Climatic trends in Puerto Rico: observed and projected since 1980. *Clim. Res.*, **66**, 113-123.

Loughnan, M., Tapper, N., Phan, T., 2014: Identifying Vulnerable Populations in Subtropical Brisbane, Australia: A Guide for Heatwave Preparedness and Health Promotion. *Hindawi Publishing Corporation ISRN Epidemiology*, **2014**, Article ID 821759, 12 pages http://dx.doi.org/10.1155/2014/821759

Méndez-Lázaro P., O. Martínez-Sánchez, R. Méndez-Tejeda, E. Rodríguez, E. Morales, N. Schmitt-Cortijo, 2015: Extreme Heat Events in San Juan Puerto Rico: Trends and Variability of Unusual Hot Weather and its Possible Effects on Ecology and Society. *J Climatol. Weather Forecasting* 3:135. doi:10.4172/2332-2594.1000135.

Menne M.J., C.N. Williams Jr., R.S. Vose, 2009: The U.S. Historical climatology network monthly temperature data, version 2. *Bulletin of the American Meteorological Society*,**90**(7), 993-1007.

MetOffice, 2015. This Web site was accessed on May 1, 2015. [http://www.metoffice.gov.uk/learning/learn-about-the-weather/weather phenomena/heatwave.]

NCEI, 2016: The National Centers for Environmental Information. Accessed on February 20, 2016, [Available online at https://gis.ncdc.noaa.gov/map/viewer/#app=cdo].

NCEP, 2016: The National Centers for Environmental Prediction. Accessed on February 20, 2016, [Available online at http://www.esrl.noaa.gov/ psd/data/gridded/data.ncep. reanalysis.html].

NOAA/NWS, 2016: Weather-Ready Nation. Accessed January 22, 2016. [Available online at http://www.nws.noaa.gov/com/weatherreadynation/heat_article.html#.VqKrLUn2b5p].

NOAA/ONI, 2017: Oceanic Niño Index. Accessed June 14, 2017. [http://ggweather.com/enso/oni.htm]

NWS/NOAA, 2017: Heat watch and warning. Accessed June 5, 2017. [Available online at http://www.nws.noaa.gov/om/heat/ww.shtml]

NWS, 2016: What is the heat index?. Accessed January 22, 2016. [Available online at http://www.srh.noaa.gov/ama/?n=heatindex].

OSHA, 2016: Heatillness in outdoor workers. Accessed in July 24, 2016. [Available online at https://www.osha.gov/SLTC/heatillness/index.html]

Peterson, T.C., and Coauthors, 1998a: homogeneity adjustments of in situ atmospheric climate data: a review. *Int. J. Climatol.*, **18**, 1493-1517.

Peterson, T.C., R. Vose, R. Schmoyer, and V. Razuvaev, 1998b: Global Historical Climatology Network (GHCN) Quality Control of Monthly Temperature Data. *Int. J. Climatol*, **18**, 1169-1179.

Portier CJ, Thigpen TK, Carter SR, Dilworth CH, Grambsch AE et al, 2010: *A Human Health Perspective On Climate Change: A Report Outlining the Research Needs on the Human Health Effects of Climate Change*. Research Triangle Park, NC, USA, 80 pp.

Rakib, Z.B., 2013: Extreme Temperature Climatology and Evaluation of Heat Index in Bangladesh During 1981-2010. *Journal of Presidential University*, Part: B, **2**, No.2, July 2013, 84-95.

Reeves, J., J. Chen, X.L. Wang, R. Lund, Q. Lu, 2007: A Review and Comparison of Changepoint Detection Techniques for Climate Data. *J. Appl. Meteor. Climatol.*, **46**, 900-915.

Robinson, P.J., 2000: On the definition of a heat wave. *Journal of Apply Meteorology*, **40**, 762-775.

Rohatgi, V.K., 1976: *An introduction to probability theory and mathematical statistics*. John Wiley and Sons, 684 pp.

Rothfusz, L. P. 1990. The heat index "equation" (or, more than you ever wanted to know about heat index). NWS Tech. Attachment SR 90-23, 2 pp.

Steadman, R.G., 1979: The assessment of sultriness. Part I: A temperature-humidity index based on human physiology and clothing science. *J. Appl. Meteor.*, **18**, 861-873.

Trenberth, K.E.,P.D. Jones, P. Ambenje, R. Bojariu, D. Easterling, A. Klein Tank, D. Parker, F. Rahimzadeh, J.A. Renwick, M. Rusticucci, B. Soden and P. Zhai, 2007: Observations: Surface and Atmospheric Climate Change. In: Climate Change 2007: The Physical Science Basis. Contribution of Working Group I to the Fourth Assessment Report of the Intergovernmental Panel on Climate Change [Solomon, S., D. Qin, M. Manning, Z. Chen, M. Marquis, K.B. Averyt, M. Tignor and H.L. Miller (eds.)]. Cambridge University Press, Cambridge, United Kingdom and New York, NY, USA.

Ultsch, A., and F. Roske, 2002: Self-organizing feature maps predicting sea levels. *Information Sciences*, **144**, 91–125.

638 Wang, X.Y., and Coauthors, 2012: The impact of heatwaves on mortality and emergency hospital
639 admissions from non-external causes in Brisbane, Australia. *Occup. Environ. Med*. 2012;
640 69:163e169. doi:10.1136/oem.2010.062141 169
641 Yip, Z. K.and Yau, M.K., 2012: Application of Artificial Neural Networks on North Atlantic
642 Tropical Cyclogenesis Potential Index in Climate Change. *AMS Journals online*. [Available
643 online at http://journals.ametsoc.org/doi/full/10.1175/JTECH-D-11-00178.1]
644 Zaman M., G. Fang, K. Mehmood and M. Saifullah, 2015: Trend Change Study of Climate
645 Variables in Xin'anjiang-Fuchunjiang Watershed, China. *Advances in Meteorology*, **2015**,
646 Article ID 507936, 13 pages.
647

Tables

Table 1. Characteristics of the Caribbean and Mesoamerica stations

Station name (Country)	Latitude (°N)	Longitude (°W)	Elevation (m)	Original data (days)	Filtered data (days)	Average air temperature T_{max} (°C)	Average relative humidity, RH (%)	Average H_i (°C)	*Difference* $H_i - T_{max}$ *(°C)*
1. Robert L. Bradshaw **St Kitts and Nevis**	17.311	62.719	51.8	95% 12101	93% 11888	29.3	68.5	33.4	4.1
2. V.C. Bird **Antigua & Barbuda**	17.137	61.793	18.9	95% 12203	94% 12025	29.4	67.4	33.2	3.8
3. Le Raizet **Guadeloupe**	16.265	61.532	11	71% 9068	67% 8584	29	69.8	32.8	3.8
4. Le Lamentin **Martinique**	14.591	61.003	4.9	90% 11509	89% 11341	29.9	66.2	33.9	4
5. E.T. Joshua **St. Vincent**	13.144	61.211	20.1	85% 10920	84% 10754	29.7	68.6	34	4.3
6. San Juan Intl. **Puerto Rico**	18.417	66.000	4	99% 12630	97% 12454	29.7	64.8	33.4	3.7
7. Cibao Intl. **Dominican Republic**	19.406	70.605	172.2	89% 11441	87% 11189	30.4	57.9	33.2	2.8
8. Sangster Intl. **Jamaica**	18.504	77.913	1.2	99% 12627	94% 12052	30.1	68.1	35	4.9
9. Toussaint Louverture I. **Haiti**	18.580	72.293	37.2	80% 10245	73% 9305	32	51.4	34.8	2.8
10. Goloson Intl. **Honduras**	15.742	86.853	14.9	95% 12150	87% 11116	29.5	69.6	34.1	4.6
11. Jose Marti **Cuba**	22.989	82.409	64	97% 12391	95% 12132	29.2	60.3	32.1	2.9
12. Miami Intl. **United States**	25.791	80.316	8.8	99% 12695	97% 12382	28.6	57.3	31	2.4
13. La Chinita Intl. **Venezuela**	10.558	71.728	71.6	92% 11768	89% 11437	32.8	58.1	38.3	5.5
14. Ernesto Cortissoz **Colombia**	10.890	74.781	29.9	99% 12669	95% 12224	31.7	65	37.9	6.2
15. Valladolid **Mexico**	20.683	88.200	27	90% 11513	88% 11344	30.7	62	35.1	4.4

652 Table 2. The climate characteristics of the Mesoamerican and Caribbean zones.

Zone	Average filtered data	Average air temperature, T_{max} (°C)	Average relative humidity, RH (%)	Average H_i (°C)	Average difference $(H_i - T_{max})$ (°C)
Lesser Antilles	87% 11160	29.4	68.1	33.5	4.1
Greater Antilles	94% 12026	29.9	61.3	33.3	3.4
Mesoamerican coastal zone	93.7% 11984	31.7	61.7	37.1	5.4

653

654 Table 3. Trends and p-values for Lesser and Greater Antilles, and Mesoamerica zones.

Zone	Maximum air temperature		Maximum daytime H_i		Relative Humidity	
	Slope (°C year^{-1})	p-value	Slope (°C year^{-1})	p-value	Slope (% year^{-1})	p-value
Lesser Antilles	0.02	0.00	0.04	0.00	-0.09	0.00
Greater Antilles	0.01	0.29	0.02	0.27	0.02	0.22
Mesoamerica	0.06	0.00	0.16	0.00	-0.00	0.92

655

656 Table 4. Heat index extreme events per station and per percentile.

Station **(Country)**	HI Extreme Events 95 Percentile	HI Extreme Events 96 Percentile	HI Extreme Events 97 Percentile	HI Extreme Events 98 Percentiles	HI Extreme Events 99 Percentile
Robert L. Bradshaw (**St Kitts and Nevis)**	12	4	3	2	1
V.C. Bird (**Antigua & Barbuda)**	14	12	10	4	3
Le Raizet (**Guadalupe)**	4	2	0	0	0
Le Lamentin (**Martinique)**	2	2	1	1	0
E.T. Joshua (**St. Vincent)**	10	9	1	0	0
San Juan Intl. (**Puerto Rico)**	11	8	4	3	0
Cibao Intl. (**Dominican Republic)**	6	4	1	0	0
Sangster Intl (**Jamaica)**.	18	10	5	0	0
Toussaint Louverture Intl.(**Haiti)**	10	6	2	2	0
Goloson Intl. (**Honduras)**	9	7	2	1	1
Jose Marti (**Cuba)**	2	1	1	1	0
Miami Intl. (**United States)**	17	9	6	3	1
La Chinita Intl. (**Venezuela)**	14	9	6	4	3
Ernesto Cortissoz (**Colombia)**	5	3	3	1	1
Valladolid (**Mexico)**	10	0	0	0	0
Total HI Extreme Events	**144**	**86**	**45**	**22**	**10**

657

658 Table 5. Heat index thresholds for station

Station **(Country)**	Thresholds (97th percentile)		Average	Average	Difference of thresholds
	Min (ºC)	Max (ºC)	Min (ºC)	Max(°C)	(°C)
1. Robert L. Bradshaw (**St Kitts and Nevis)**	31.1	38.7	30.7	38.8	8.1
2. V.C. Bird (**Antigua & Barbuda)**	31.5	38.2			
3. Le Raizet (**Guadeloupe)**	29	38.8			
4. Le Lamentin (**Martinique)**	30.2	39.1			
5. E.T. Joshua (**St. Vincent)**	31.7	39			
6. San Juan Intl (**Puerto Rico)**	30.1	39.5	27.7	40.2	12.5
7. Cibao Intl (**Dominican Republic)**	23.9	39.6			
8. Sangster Intl (**Jamaica)**	30.9	42.3			
9. Toussaint Louverture Intl (**Haiti)**	28.7	40.3			
10. Goloson Intl. (**Honduras)**	24.6	41.1			
11. Jose Marti (**Cuba)**	24.5	40			
12. Miami Intl (**United States)**	31.2	38.7			
13. La Chinita Intl. (**Venezuela)**	31.9	45.2	28.5	46.0	17.5
14. Ernesto Cortissoz (**Colombia)**	31.9	43.2			
15. Valladolid (**Mexico)**	21.7	49.7			

659

660

661

662 Table 6. Bivariate and marginal probability distributions of the HIEE.

$f_{D,RI}(d,ri)$		ri (°C)					$f_D(d)$
		1	*2*	*3*	*4*	*5*	
d (days)	*2.0*	0.1111	0.2222	0.0889	0.0222	0.0444	**0.4889**
	2.5	0.1111	0.1111	0.0222	0.0444	0.0444	**0.3333**
	3.0	0	0.0222	0.0222	0	0	**0.0444**
	3.5	0.0222	0	0.0667	0.0222	0	**0.1111**
	4.0	0	0	0	0	0	**0**
	4.5	0	0	0	0.0222	0	**0.0222**
$f_{RI}(ri)$		**0.2444**	**0.3556**	**0.2**	**0.1111**	**0.0889**	

663

664

665 **Figures Caption List**
666

667 Figure 1. Location of the Mesoamerica and Caribbean Region. The numbers indicate the name
668 and location of the selected stations, and the red dashes indicate the homogeneous regions
669 associated with Greater and Lesser Antilles Islands.

670 Figure 2. Panels a) and b) show the original and filtered data for station located in Antigua and
671 Barbuda. Panels c) and d) exhibit the original and filtered data for station located in Cuba, and
672 similarly, panels e) and d) show the original and filtered data for station located in Venezuela.
673 These are examples of stations located in Lesser, and Greater Antilles, and Mesoamerica,
674 respectively.

675 Figure 3. Panels a), b) and c) show the climatology of air temperature, heat index, and relative
676 humidity. Panels d), e) and f) show the average of air temperature, heat index and relative
677 humidity. Panel g) exhibits the trends spatial distribution of head index. Climatology, grid
678 averages and grid trends were computed using 6-hour NCEP data during 35-year period (1980-
679 2014).

680 Figure 4. Panels a), b) and c) show the 24-hour climatology of air temperature, heat index and
681 relative humidity for stations located in Antigua & Barbuda, Puerto Rico and Colombia,
682 respectively. The time is given in UTC and these figures show the averages of hourly 35-year
683 data.

684 Figure 5. Panels a), b) and c) show the trends of maximum air temperature, maximum heat index
685 and relative humidity, respectively. Panels d), e) and f) exhibit the climatology of relative
686 humidity, maximum air temperature and maximum heat index, respectively. Panel g) shows the

687 difference of two-climatology variables the maximum heat index, and maximum air temperature.
688 The relative humidity presented in this figure is the one that correspond to the hourly maximum
689 air temperature.

690 Figure 6. The top, central and bottom panels show the trends of the maximum air temperature for
691 the Lesser and Greater Antilles, and Mesoamerica zones.

692 Figure 7. The top, central and bottom panels show the trends of maximum heat index for the
693 Lesser and Greater Antilles, and Mesoamerica zones.

694 Figure 8. The top, central and bottom panels show trends of the relative humidity associated to
695 the maximum air temperature for the Lesser and Greater Antilles, and Mesoamerica zones.

696 Figure 9. Monthly climatology based on daily maximum air temperature, daily maximum heat
697 index, and daily relative humidity associated to the maximum air temperature.

698 Figure 10. Bivariate probability distribution of duration and relative intensity of heat index
699 extreme events.

700 Figure 11. Panel (a) shows the annual and (b) panel exhibits the monthly frequency of heat
701 index extreme events

702

703

Figures

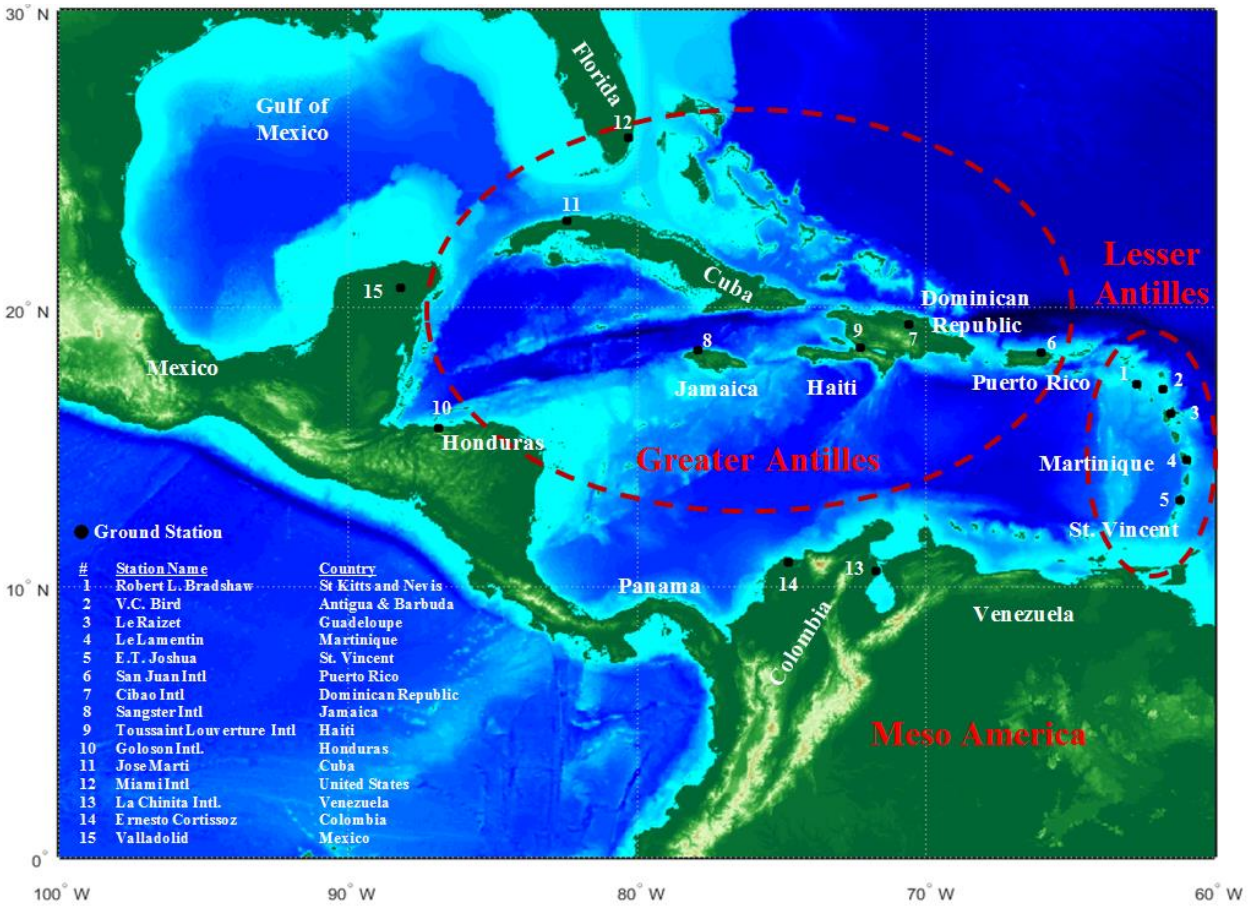

Figure 1. Location of the Mesoamerica and Caribbean Region. The numbers indicate the name and location of the selected stations, and the red dashes indicate the homogeneous regions associated with Greater and Lesser Antilles Islands.

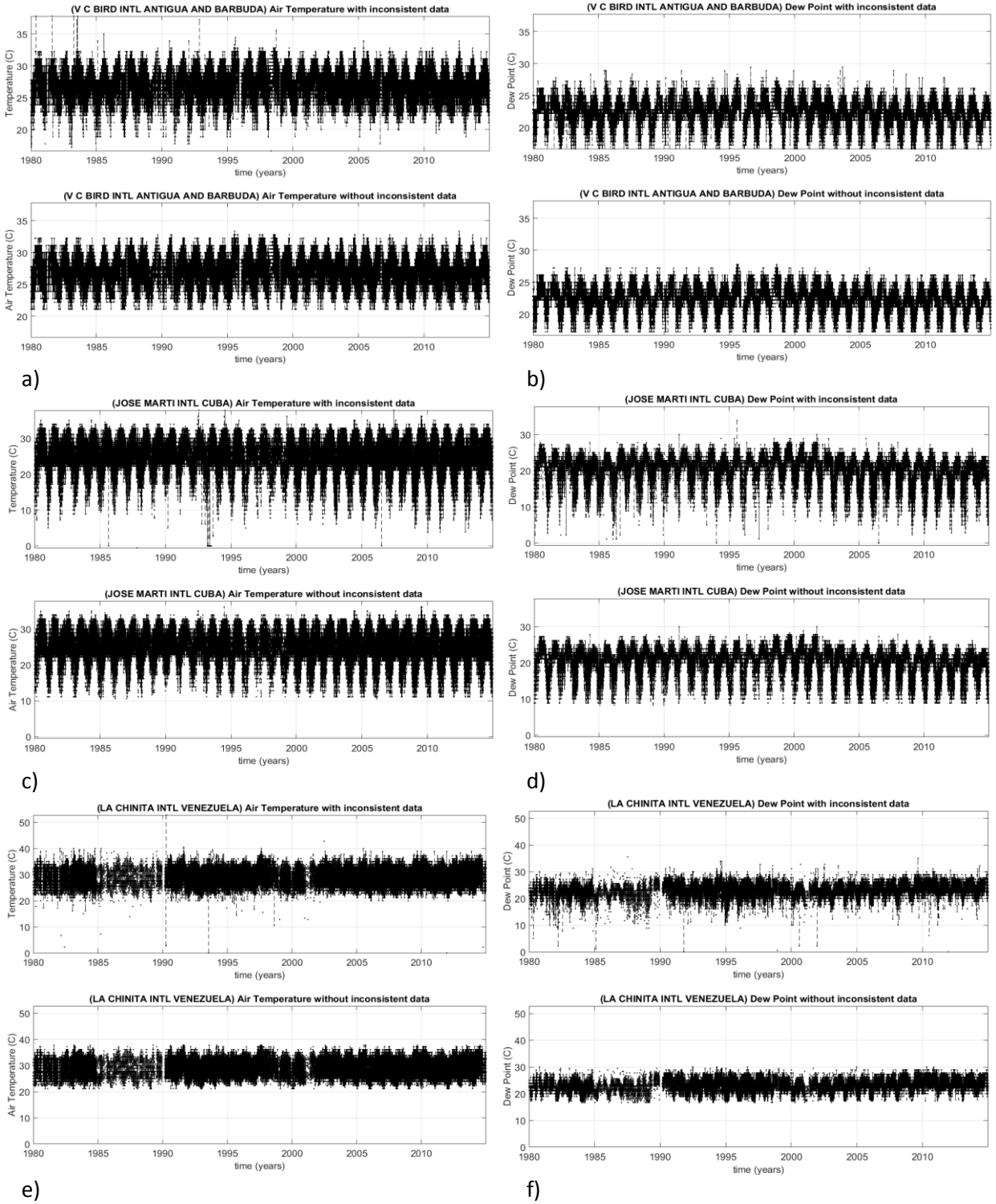

Figure 2. Panels a) and b) show the original and filtered data for station located in Antigua and Barbuda. Panels c) and d) exhibit the original and filtered data for station located in Cuba, and similarly, panels e) and d) show the original and filtered data for station located in Venezuela. These are examples of stations located in Lesser, and Greater Antilles, and Mesoamerica, respectively.

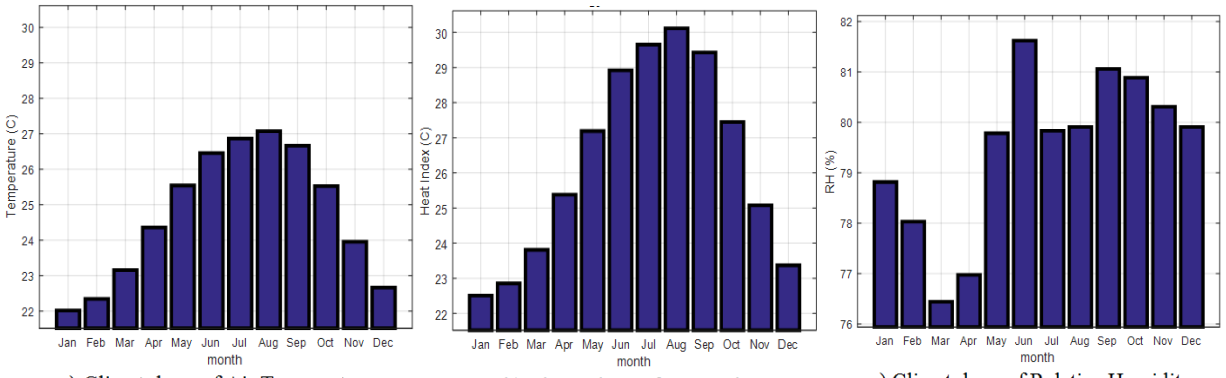

722 a) Climatology of Air Temperature b) Climatology of Heat Index c) Climatology of Relative Humidity

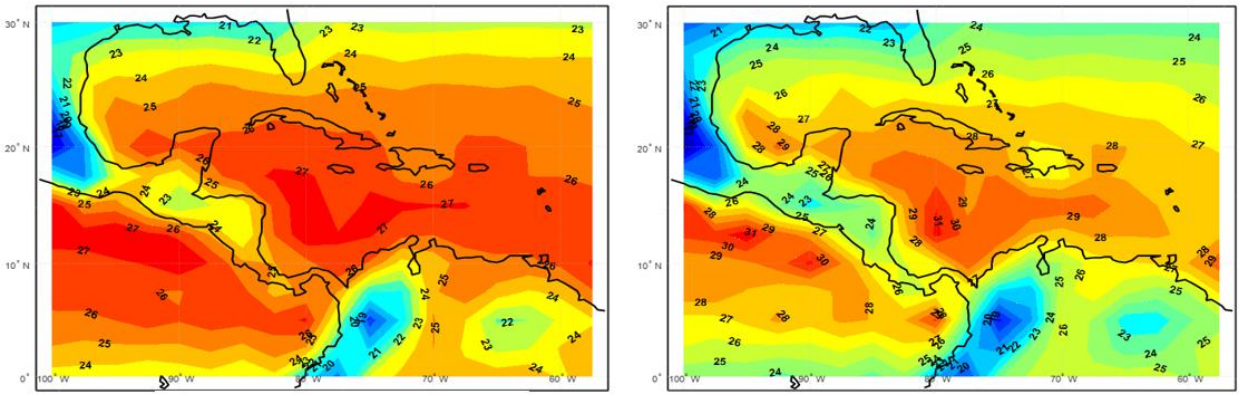

723 d) Average of Air Temperature e) Average of Heat Index

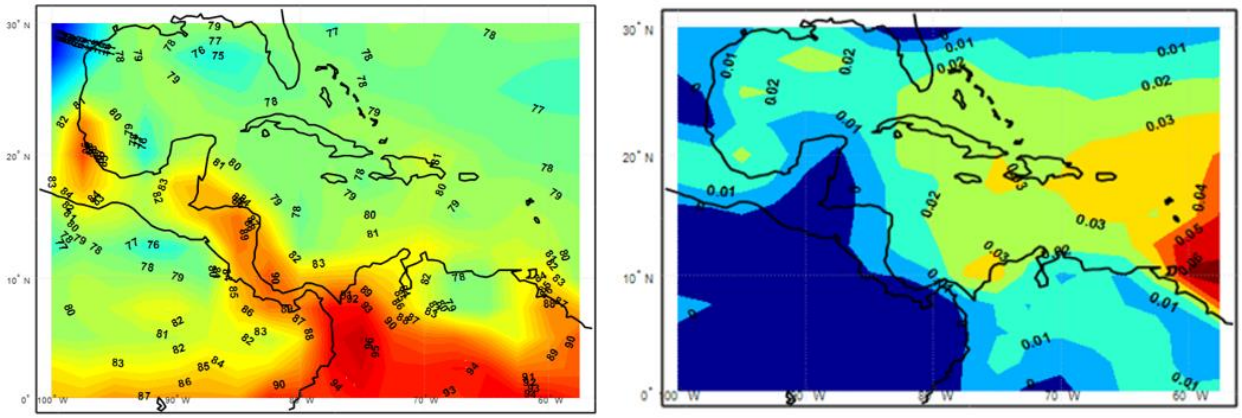

724 f) Average of Relative Humidity g) Trends of Heat Index

725 Figure 3. Panels a), b) and c) show the climatology of air temperature, heat index, and relative
726 humidity. Panels d), e) and f) show the average of air temperature, heat index and relative
727 humidity. Panel g) exhibits the trends spatial distribution of head index. Climatology, grid
728 averages and grid trends were computed using 6-hour NCEP data during 35-year period (1980-
729 2014).
730

731

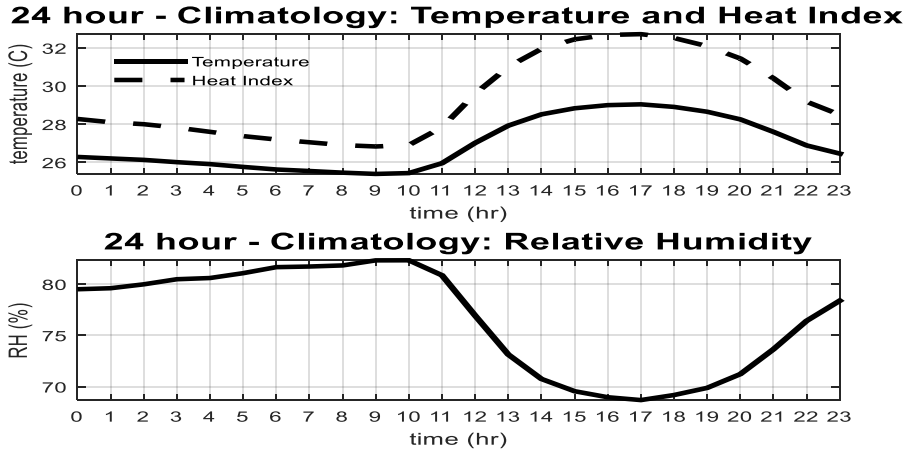

732
733 **(a) Antigua & Barbuda Station**

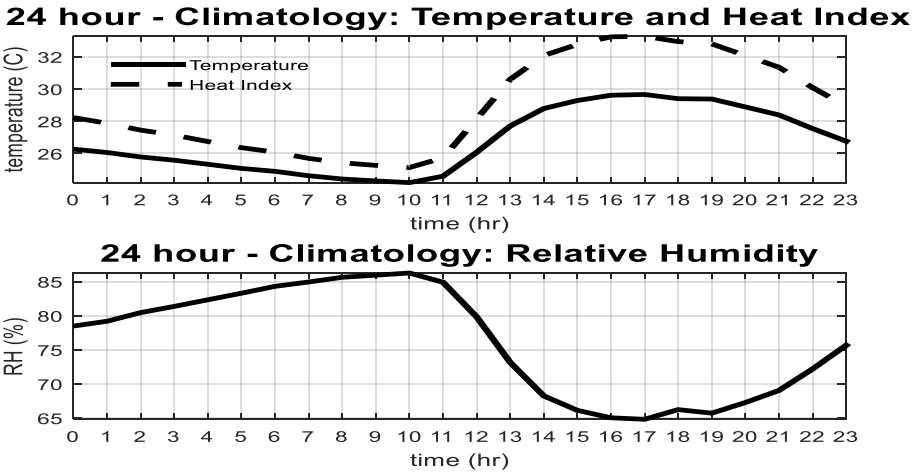

734
735 **(b) Puerto Rico Station**
736

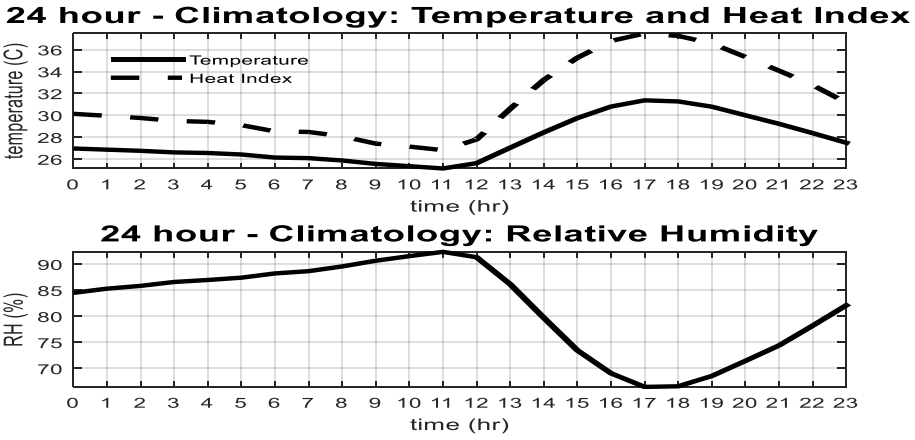

737
738 **(c) Colombia Station**
739

740 Figure 4. Panels a), b) and c) show the 24-hour climatology of air temperature, heat index and
741 relative humidity for stations located in Antigua & Barbuda, Puerto Rico and Colombia,
742 respectively. The time is given in UTC and these figures show the averages of hourly 35-year
743 data.

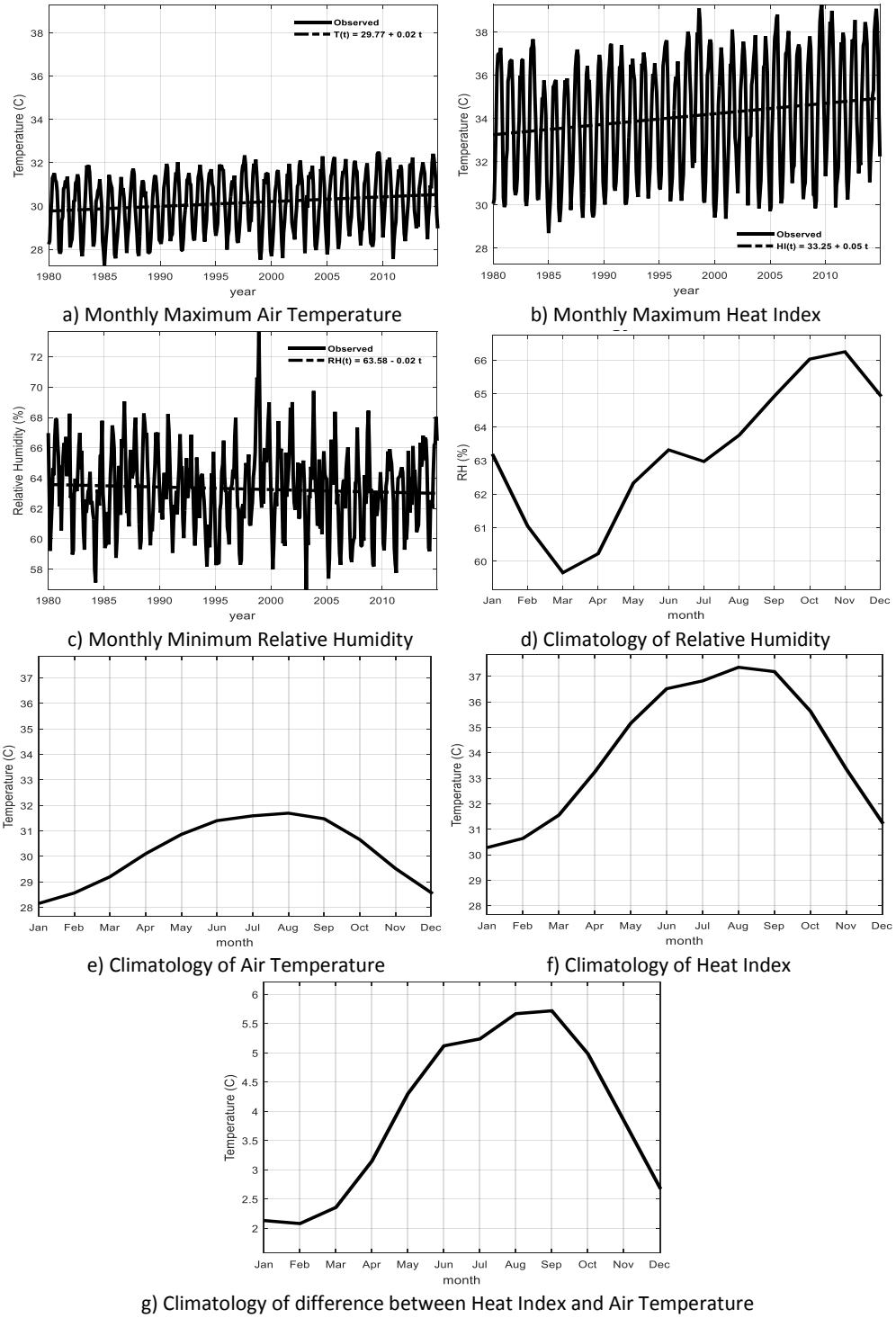

Figure 5. Panels a), b) and c) show the trends of maximum air temperature, maximum heat index and relative humidity, respectively. Panels d), e) and f) exhibit the climatology of relative humidity, maximum air temperature and maximum heat index, respectively. Panel g) shows the difference of two-climatology variables the maximum heat index, and maximum air temperature. The relative humidity presented in this figure is the one that correspond to the hourly maximum air temperature.

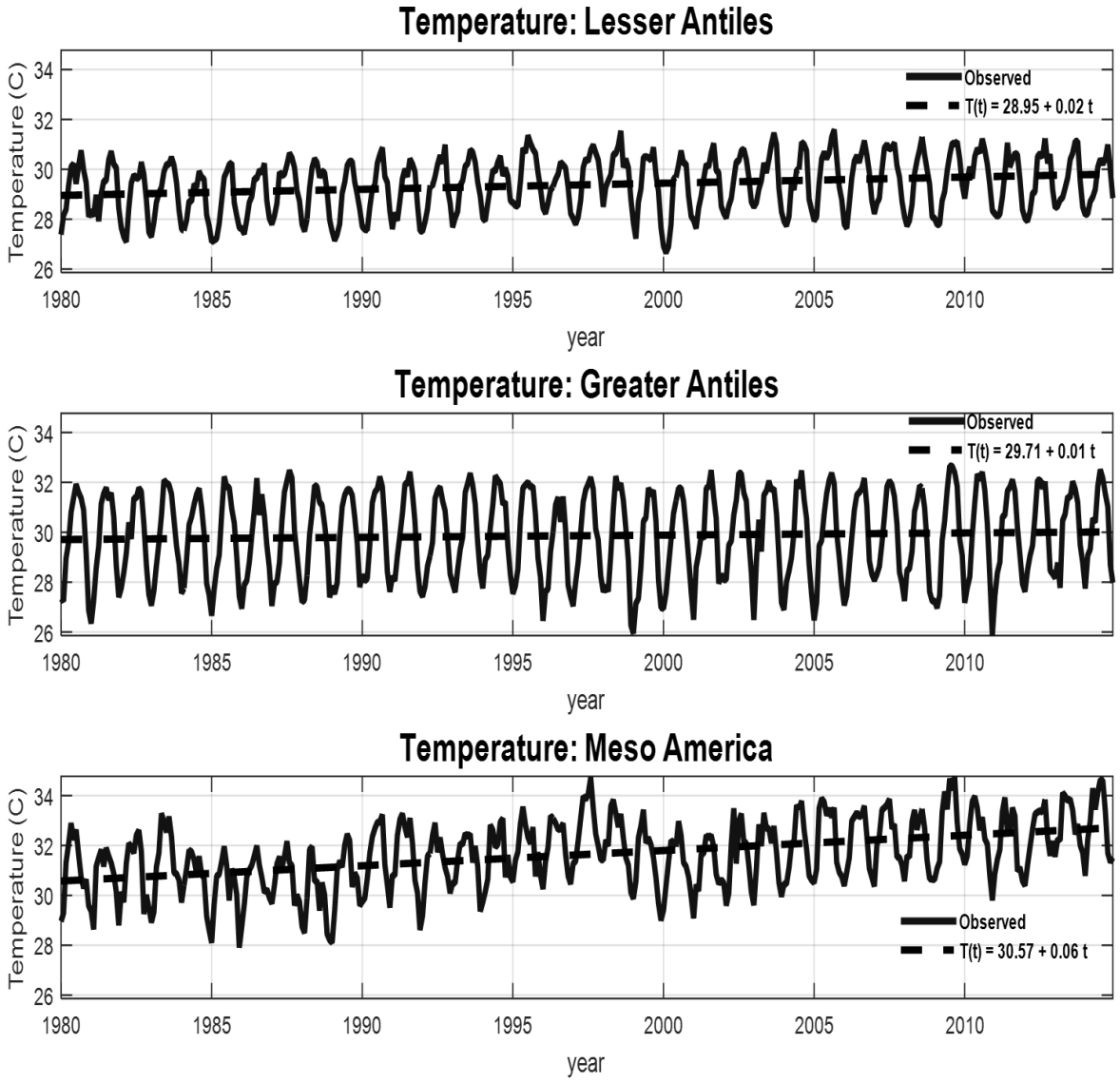

758

759 Figure 6. The top, central and bottom panels show the trends of the maximum air temperature for

760 the Lesser and Greater Antilles, and Mesoamerica zones.

761

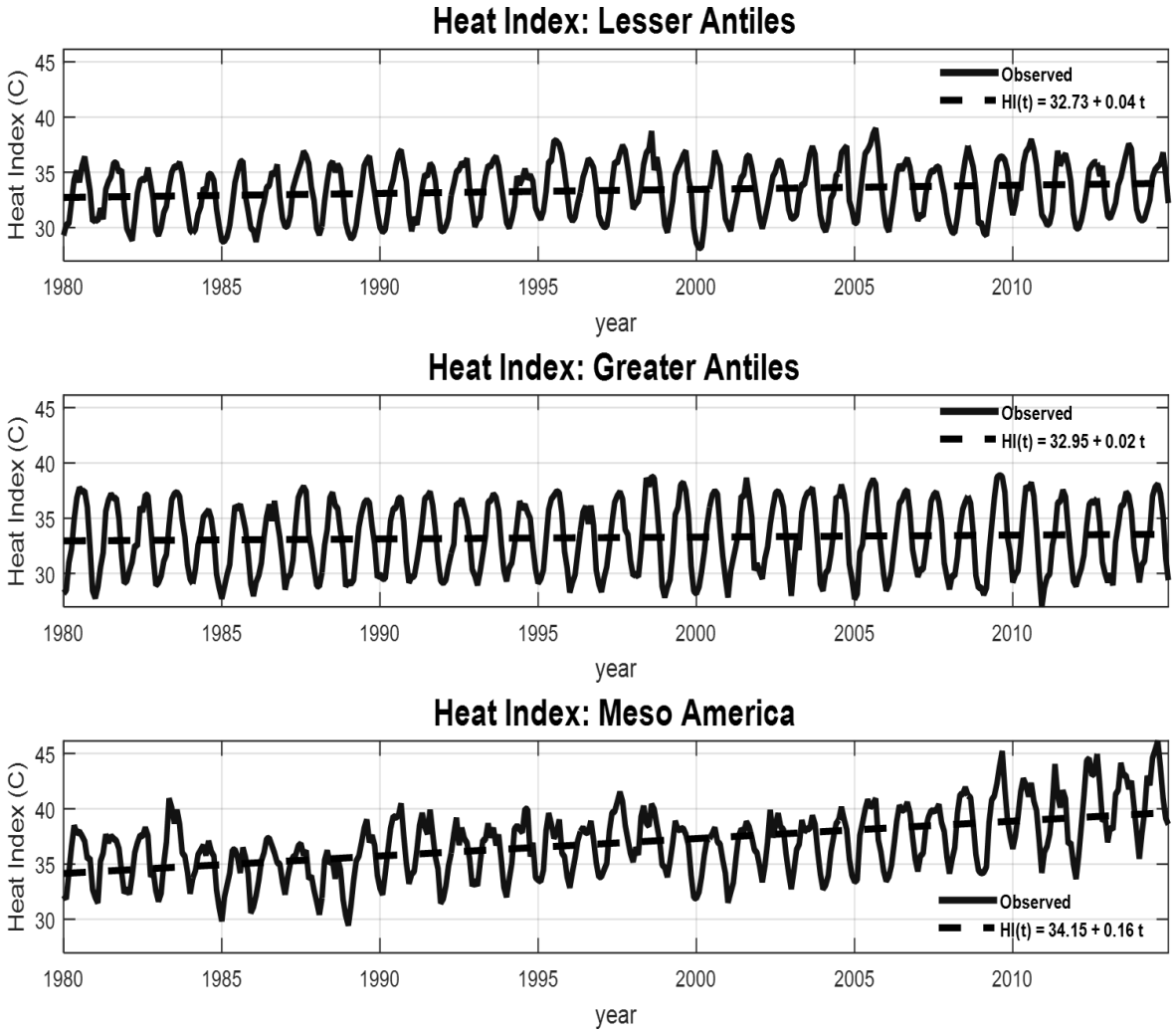

762

763 Figure 7. The top, central and bottom panels show the trends of maximum heat index for the
764 Lesser and Greater Antilles, and Mesoamerica zones.

765

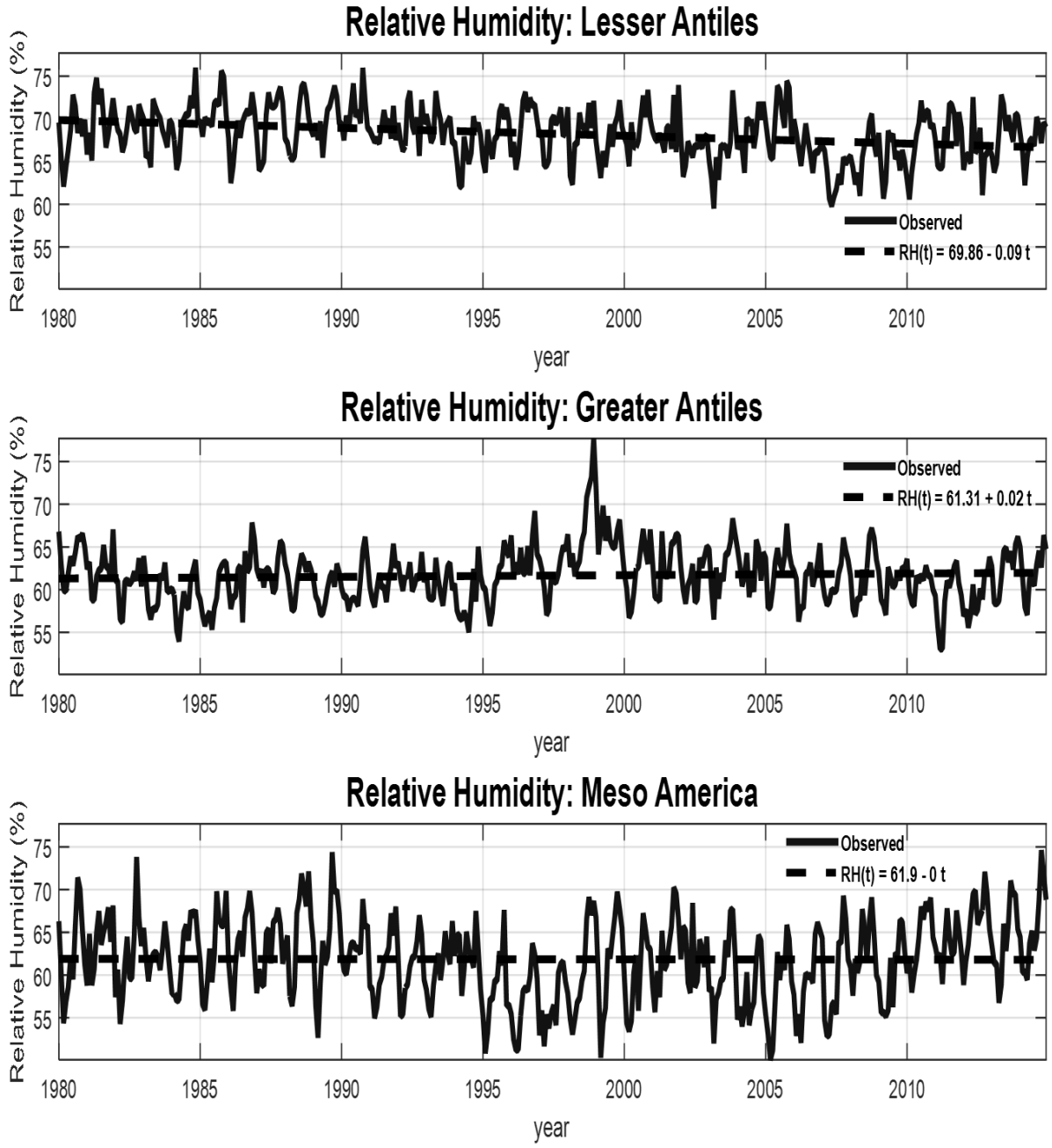

Figure 8. The top, central and bottom panels show trends of the relative humidity associated to the maximum air temperature for the Lesser and Greater Antilles, and Mesoamerica zones.

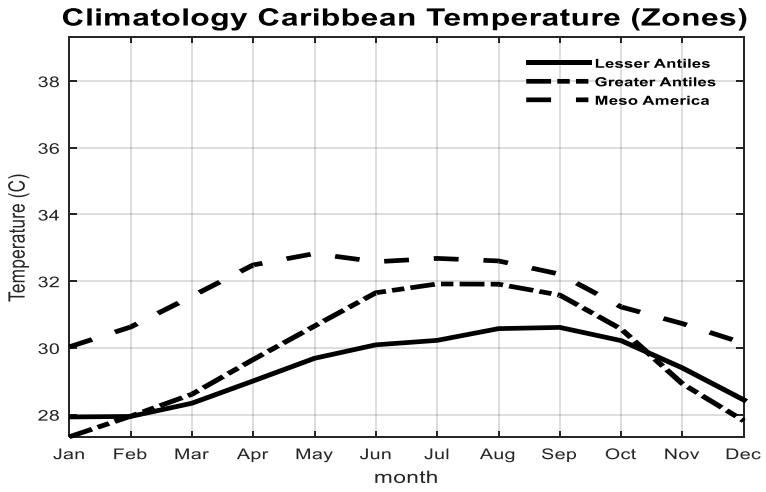

770

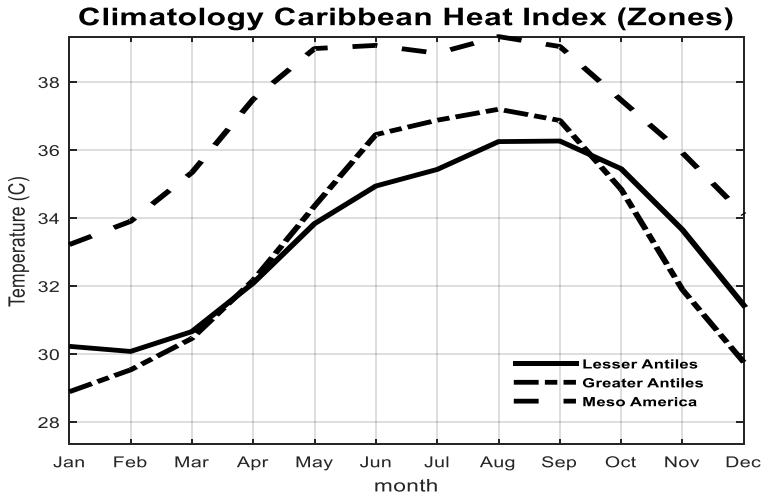

771

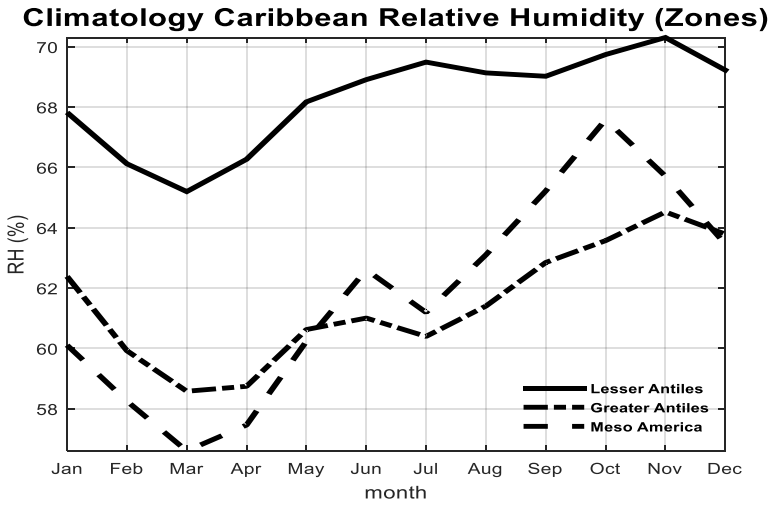

772

773 Figure 9. Monthly climatology based on daily maximum air temperature, daily maximum heat

774 index, and daily relative humidity associated to the maximum air temperature.

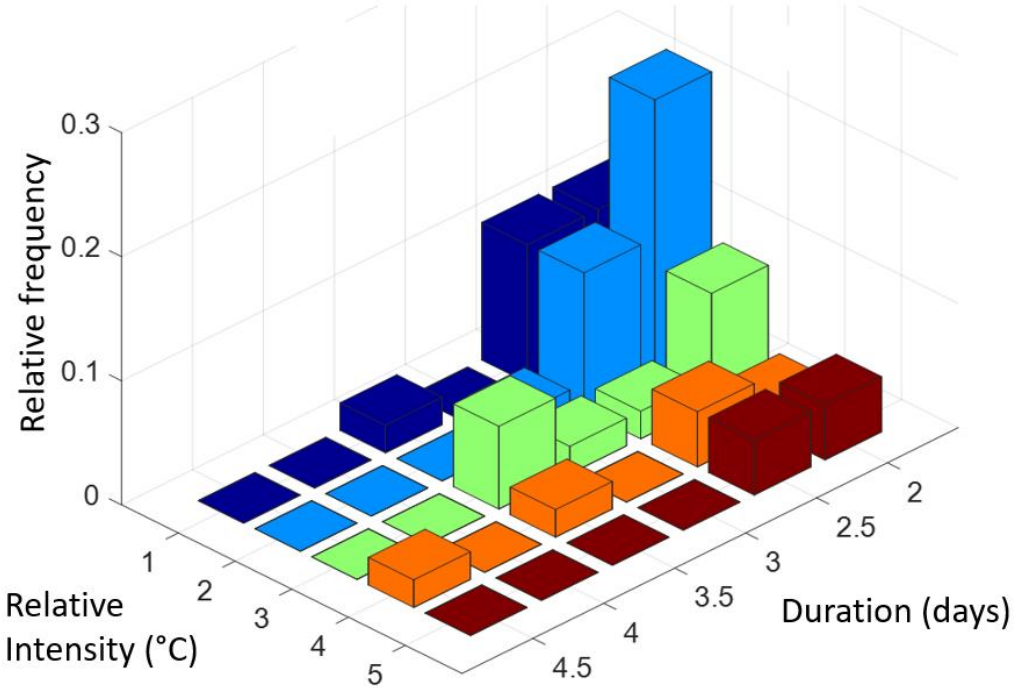

Figure 10. Bivariate probability distribution of duration and relative intensity of heat index extreme events.

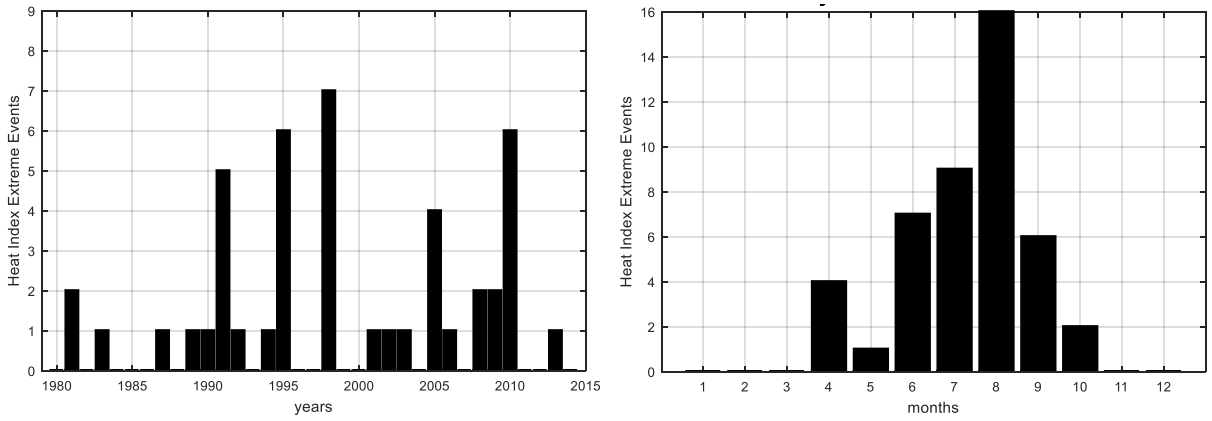

(a) (b)

Figure 11. Panel (a) shows the annual and panel (b) exhibits the monthly frequency of heat index extreme events